Scatterometer-Based Assessment of 10-m Wind Analyses from the Operational ECMWF and NCEP Numerical Weather Prediction Models

DUDLEY B. CHELTON AND MICHAEL H. FREILICH

College of Oceanic and Atmospheric Sciences, Oregon State University, Corvallis, Oregon

ABSTRACT

Wind measurements by the National Aeronautics and Space Administration (NASA) scatterometer (NSCAT) and the SeaWinds scatterometer on the NASA QuikSCAT satellite are compared with buoy observations to establish that the accuracies of both scatterometers are essentially the same. The scatterometer measurement errors are best characterized in terms of random component errors, which are about 0.75 and 1.5 m s^{-1} for the along-wind and crosswind components, respectively.

The NSCAT and QuikSCAT datasets provide a consistent baseline from which recent changes in the accuracies of 10-m wind analyses from the European Centre for Medium-Range Weather Forecasts (ECMWF) and the U.S. National Centers for Environmental Prediction (NCEP) operational numerical weather prediction (NWP) models are assessed from consideration of three time periods: September 1996–June 1997, August 1999–July 2000, and February 2002–January 2003. These correspond, respectively, to the 9.5-month duration of the NSCAT mission, the first 12 months of the QuikSCAT mission, and the first year after both ECMWF and NCEP began assimilating QuikSCAT observations. There were large improvements in the accuracies of both NWP models between the 1997 and 2000 time periods. Though modest in comparison, there were further improvements in 2002, at least partly attributable to the assimilation of QuikSCAT observations in both models.

There is no evidence of bias in the 10-m wind speeds in the NCEP model. The 10-m wind speeds in the ECMWF model, however, are shown to be biased low by about 0.4 m s^{-1}. While it is difficult to eliminate systematic errors this small, a bias of 0.4 m s^{-1} corresponds to a typical wind stress bias of more than 10%. This wind stress bias increases to nearly 20% if atmospheric stability effects are not taken into account. Biases of these magnitudes will result in significant systematic errors in ocean general circulation models that are forced by ECMWF winds.

---

1. Introduction

Quantitative assessment of 10-m wind fields obtained from operational numerical weather prediction (NWP) models has long been limited by the lack of suitable validation data. The dense and global coverages afforded by the National Aeronautics and Space Administration (NASA) scatterometer (NSCAT) launched on the Japanese ADEOS satellite and the SeaWinds scatterometer onboard the QuikSCAT satellite provide unique opportunities to quantify the accuracies of recent and contemporary NWP 10-m wind analyses. The combined NSCAT and QuikSCAT datasets are used here to assess the 10-m wind analyses from the operational NWP models at the European Centre for Medium-Range Weather Forecasts (ECMWF) and the U.S. National Centers for Environmental Prediction

(NCEP). The objective is to investigate the changes in the accuracies of the 10-m wind analyses from these NWP models over the time period September 1996–January 2003 based on comparisons with the NSCAT and QuikSCAT observations of 10-m winds.

The fundamentals of scatterometry and the differences between the NSCAT and QuikSCAT scatterometer systems are summarized in sections 2a–e. To establish these two datasets as a consistent baseline against which ECMWF and NCEP winds can be compared, it is shown in section 2f from comparisons with buoy observations that the measurement errors are essentially the same for the two scatterometers. It is further shown in section 3 that the effects of atmospheric stability on the comparisons between the NWP and scatterometer winds are of secondary importance. Temporal changes in the statistics of the differences between the scatterometer and NWP winds can therefore be attributed primarily to changes in the accuracies of the NWP wind analyses.

Improvements in the accuracies of 10-m wind analyses from the operational ECMWF and NCEP models

Corresponding author address: Dudley B. Chelton, College of Oceanic and Atmospheric Sciences, Oregon State University, 104 COAS Administration Building, Corvallis, OR 97331-5503.
E-mail: chelton@coas.oregonstate.edu

are summarized from consideration of root-mean-square (rms) component differences in section 4 and wind speed differences in section 5 for three different time periods: 1) September 1996–June 1997, which corresponds to the 9.5-month duration of the NSCAT data record; 2) August 1999–July 2000, which corresponds to the first 12 months of the QuikSCAT mission; and 3) February 2002–January 2003. During the first two time periods, neither ECMWF nor NCEP assimilated NSCAT or QuikSCAT data into their operational models; the two scatterometer datasets thus provide entirely independent assessments of the qualities of the NWP 10-m wind analyses. NCEP and ECMWF began assimilating QuikSCAT data operationally on 13 and 22 January 2002, respectively.[1] The third time period therefore corresponds to the first 12 months of QuikSCAT assimilation in both NWP models, providing an assessment of the impact of scatterometer data on the accuracies of ECMWF and NCEP analyses of 10-m winds.[2]

2. Scatterometry

a. NSCAT and QuikSCAT measurement geometries

Scatterometers are spaceborne radars that infer surface winds from the roughness of the sea surface based on measurements of ocean radar backscatter cross section, denoted as σ_0, which varies with wind speed, wind direction relative to the antenna azimuth, incidence angle, polarization, and radar frequency. Near-simultaneous, collocated σ_0 measurements are acquired from different measurement geometries and polarizations, allowing wind speed and direction to be retrieved in ground processing (Naderi et al. 1991). The scatterometers developed and operated by NASA acquire vertically and horizontally polarized σ_0 measurements at Ku-band frequencies (13.995 GHz for NSCAT and 13.4 GHz for QuikSCAT) with approximately 25-km resolution. As summarized below, the antenna configurations are significantly different for NSCAT and QuikSCAT, yielding very different geometries for the collocated measurement sets.

A description of the NSCAT scatterometer, which operated for 9.5 months from September 1996–June 1997, is given by Naderi et al. (1991). The multiple antenna azimuths required for vector wind retrievals were obtained from four fixed, fan-beam antennas on each side of the spacecraft (Fig. 1). The σ_0 measurements had individual cell dimensions of about 10 km in the cross-beam direction and 60 km in the along-beam direction (Fig. 2). As the satellite traveled along its orbit, the four different antennas sampled a given location on the sea surface over a time interval of 4 min or less, depending on the distance from the satellite ground track. The set of cells with collocated centroids from all four antennas illuminated an area of approximately $(25 \text{ km})^2$ (Fig. 2). These collocated σ_0 measurements were processed to estimate vector winds across a pair of 600-km swaths separated by a 329-km gap centered on the satellite ground track. The NSCAT measurement geometry thus yielded σ_0 measurements with incidence angles that varied systematically from 17° at the inner edges of the swaths to 61° at the outer edges. The relative azimuth angles between each set of four collocated σ_0 measurements were constant across the swaths.

A description of the SeaWinds scatterometer on the QuikSCAT satellite, which has been operating since 19 July 1999, is given by Freilich et al. (1994). QuikSCAT uses a dual-beam, conically scanning antenna that samples the full range of azimuth angles during each revolution. Instantaneous backscatter measurements are obtained at fixed incidence angles of 46° and 54° (Fig. 3), with the inner and outer beams transmitting and receiving horizontally and vertically polarized radiation, respectively. Each σ_0 measurement is elliptical with characteristic dimensions of about 25×35 km (Fig. 4). The antenna revolves at a rate of ~19 rpm, and the spacecraft advances about 22 km along the ground track during each antenna revolution. While σ_0 measurements are obtained at a constant incidence angle for each beam, the relative azimuth angles between collocated backscatter measurements vary systematically with cross-track location.

At the QuikSCAT orbital altitude of 803 km, the radii of the inner and outer beams are about 700 and 900 km. In principle, the QuikSCAT measurement approach therefore yields a single, contiguous swath of 1800-km width centered on the satellite ground track. At surface locations imaged by both beams, backscatter measurements from four geometries within a time interval of less than 4.5 min can be collocated—one from each forward-looking beam and one from each aft-looking beam. Only two backscatter measurements are obtained in the outer 200 km of the swath on each side of the spacecraft (the forward- and aft-looking measurements from the outer beam). Accurate wind retrievals are restricted to the middle 1600 km of the 1800-km swath (see section 2e).

Scatterometers measure small-scale roughness, which depends on surface stress. The wind retrievals are calibrated to the equivalent neutral-stability wind at a reference height of 10 m above the sea surface—that is, the 10-m wind that would be associated with the

---

[1] As summarized in section 2c, the "Standard Product" QuikSCAT vector winds analyzed in this study differ from the "Near-Real-Time" QuikSCAT winds that are assimilated into the ECMWF and NCEP models.

[2] ECMWF began assimilating wind measurements from the scatterometers on the European Space Agency Earth Remote Sensing (ERS) satellites in January 1996 and from the U.S. Defense Meteorological Satellite Program (DMSP) Special Sensor Microwave/Imager (SSM/I) radiometers in October 1999. NCEP assimilated both ERS and the SSM/I winds throughout all three time periods considered here.
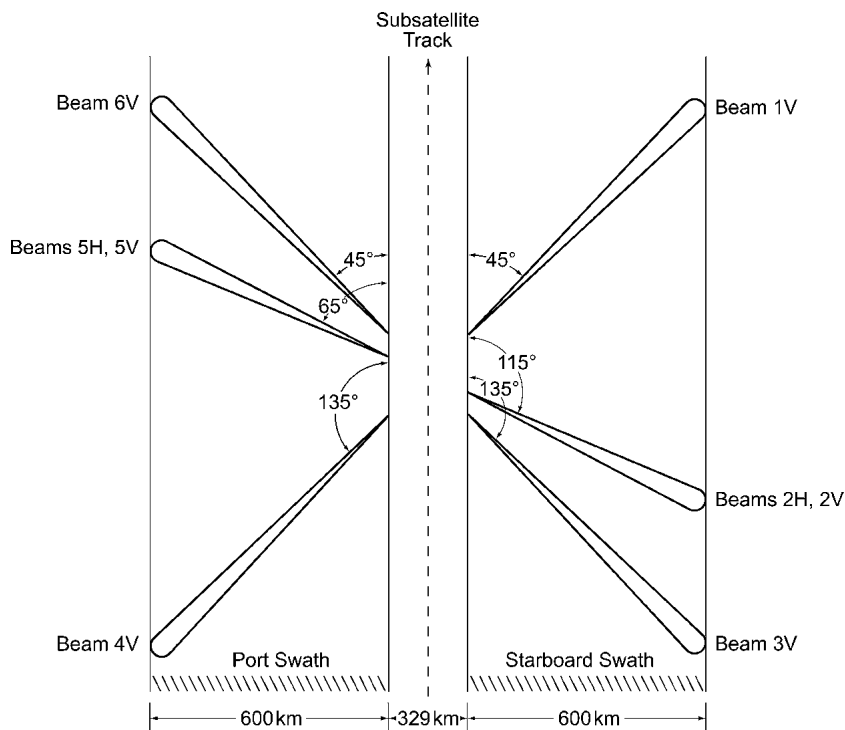
FIG. 1. Schematic plan view of the two parallel measurement swaths and the pointing directions for the three antennas of the NSCAT scatterometer system. The fore and aft antennas measure only vertical polarization, while both vertical and horizontal polarization are measured at the middle angle on each side of the spacecraft (after Naderi et al. 1991).

observed surface stress if the atmospheric boundary layer were neutrally stratified (Liu and Tang 1996). The vector wind stress and 10-m neutral-stability wind are related by a neutral-stability drag coefficient (for example, Trenberth et al. 1990; Smith 1988). The differences between observed 10-m winds and equivalent neutral-stability winds at 10 m are discussed in section 3.

The accuracy of vector winds retrieved from scatterometer data depends on accurate knowledge of the relationship between σ_0 and winds (the "model function"), the accuracy of the backscatter measurements themselves, and the geometry (most importantly, the azimuthal diversity) of the collocated data. Directional ambiguity removal errors and rain also influence the accuracy of the scatterometer estimates of wind velocity. Slightly different model functions were used for NSCAT and QuikSCAT processing, in part owing to the small difference in radar frequencies used by the instruments, and in part from adjustments made to the QuikSCAT model function to address apparent underestimates at high wind speeds from the NSCAT model function (Donnelly et al. 1999; Yueh et al. 2000).

b. Near-Real-Time versus Standard Product QuikSCAT winds

The QuikSCAT vector winds that have been assimilated into the ECMWF and NCEP models since January 2002 are the so-called Near-Real-Time (NRT) winds produced by the National Oceanic and Atmospheric Administration (NOAA). For the NRT wind product, the overlapping σ_0 measurements obtained from each of the four possible antenna geometrics (inner/outer beam and fore/aft viewing geometry) are averaged within each wind vector cell to obtain a single σ_0 estimate. Wind retrievals are then calculated from the 2–4 averaged σ_0 measurements in each wind vector cell. This preaveraging for the NRT product was performed in order to decrease the computational resources required for wind vector retrievals. The so-called Standard Product QuikSCAT winds that are analyzed in this study were produced at the Jet Propulsion Laboratory using all of the individual σ_0 measurements within each wind vector cell without preaveraging, as shown by the example in Fig. 4.

The NRT and Standard Product QuikSCAT wind datasets also differ in the details of directional ambiguity removal. Because of the need to retrieve winds in near–real time (within 3 h of acquisition by the satellite), ambiguity removal for the NRT product is initialized by the shortest possible (typically 3- or 6-h) forecast from the NCEP AVN model. For the Standard Product QuikSCAT winds analyzed here, ambiguity removal was initialized by the operational 10-m NCEP nowcast analyses.
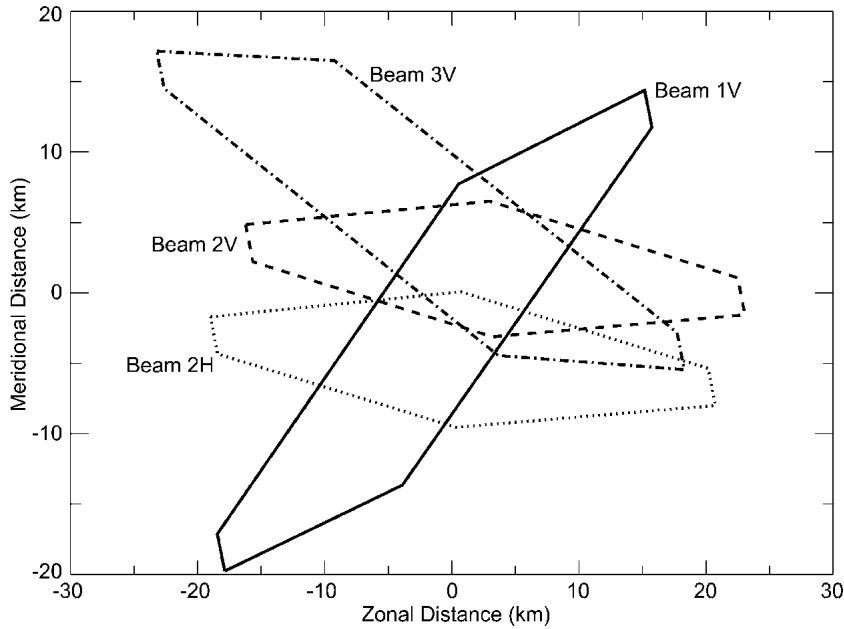
FIG. 2. Collocated 25-km NSCAT radar backscatter cells from a near-equatorial midswath location (from Chelton et al. 2000).

c. Rain effects

In nonraining conditions, spatial and temporal variations in microwave propagation through the atmosphere are negligible. In the presence of significant rain, the microwave radiation can be scattered or absorbed by raindrops in the atmosphere, and raindrops hitting the sea surface can cause centimetric roughness (and thus variations in σ_0) that is not well correlated with the surface winds. Rain contamination is larger at the Ku-band frequencies of the NSCAT and QuikSCAT instruments than at the C-band frequencies used for the scatterometers on the European Space Agency Earth Remote Sensing satellites, *ERS-1* and *ERS-2* (Tournadre and Quilfen 2003). This disadvantage in Ku-band systems is offset by the advantage of greater wind speed
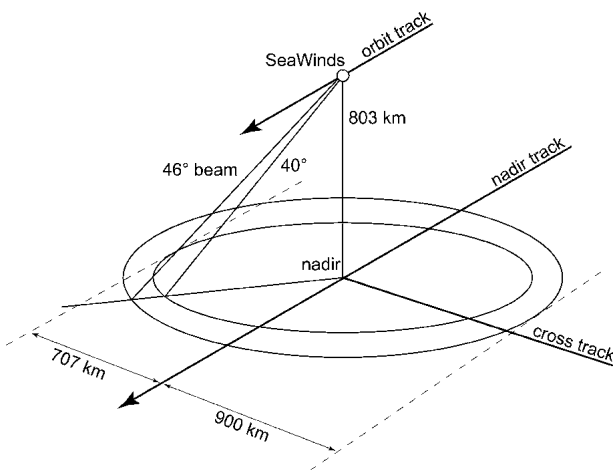

FIG. 3. Schematic plan view of the measurement swath and the measurement geometries of the two scanning antennas of the QuikSCAT scatterometer system. Antenna look angles of 40° and 46° correspond to incidence angles on the sea surface of 46° and 54° for the inner and outer beams, respectively.
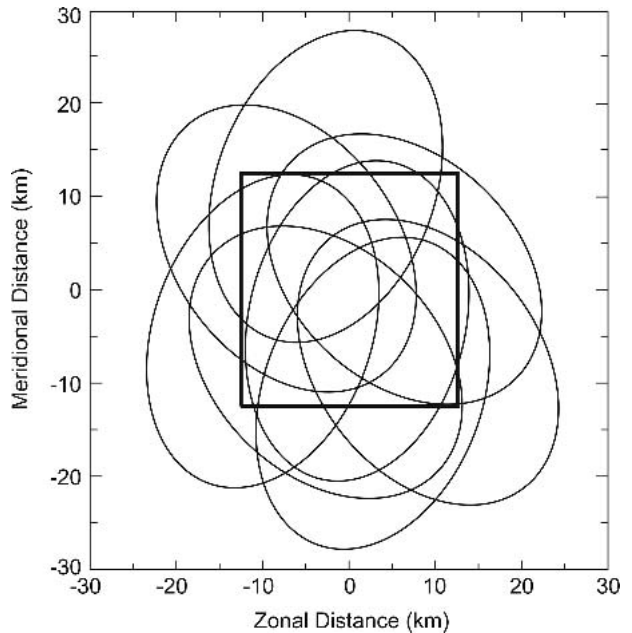

FIG. 4. Collocated QuikSCAT radar backscatter cells from a midswath location. The heavy square box denotes the 25-km square wind vector cell.

and directional sensitivity of Ku-band σ_0 (Donelan and Pierson 1987; Apel 1994).

As outlined by Mears et al. (2000), Huddleston and Stiles (2000), and Stiles and Yueh (2002), the principal manifestations of rain are 1) an increase in the measured horizontal and vertical polarization brightness temperatures at Ku-band frequencies, which increases with increasing rain rate; 2) an increase in the ratio of horizontally to vertically polarized σ_0 relative to nonraining conditions, especially at wind speeds below about 10 m s^{-1}; 3) a decrease in azimuthal modulation of σ_0 compared with nonraining conditions owing to the isotropic nature of both scattering from raindrops and the centimetric roughness caused by raindrops impinging on the sea surface; and 4) an overall increase in σ_0 relative to nonraining conditions for low wind speeds owing to scatter from raindrops in the atmosphere, and a decrease in σ_0 for higher wind speeds owing to atmospheric absorption by raindrops.

When referenced to a Cartesian coordinate system aligned with the subsatellite track, the distributions of buoy- and scatterometer-measured directions for collocated data under nonraining conditions are essentially the same (dashed lines in Fig. 5). The buoy-measured directional distribution under raining conditions (thin solid line) remains qualitatively similar to the directional distribution under nonraining conditions. However, the scatterometer-measured directional histogram under raining conditions (heavy solid line) is strongly peaked near angles of 90° and 270° relative to the satellite subtrack (that is, in the cross-track directions). For the QuikSCAT measurement geometry, the buoy comparisons thus demonstrate that rain contamination generally causes apparent wind velocities to be incorrectly oriented in the cross-track direction.

Satellite-borne passive microwave radiometers can provide quantitative estimates of rain rate (Wentz and Spencer 1998), but neither the ADEOS/NSCAT nor the QuikSCAT missions included a microwave radiometer instrument. A number of techniques for flagging

rain-contaminated observations have nonetheless been developed for QuikSCAT. Boukabara et al. (2002) and Ahmad et al. (2004, manuscript submitted to *J. Geophys. Res.*) developed empirical models relating QuikSCAT measurements of brightness temperature at 13.4 GHz (a by-product of the scatterometer σ_0 measurement approach) to rain rate. Mears et al. (2000) developed a rain flag based on the magnitudes of the "misfits" of QuikSCAT measurements of σ_0 to the model function from which wind speed and direction retrievals are calculated. For the calculations presented in this paper, a tabular, multidimensional histogram-based "MUDH" rain flag algorithm (Huddleston and Stiles 2000; see also Stiles and Yueh 2002) has been used to identify and remove all QuikSCAT wind measurements that were contaminated by rain.

A rain flag algorithm has not been developed for NSCAT. Because of the different measurement geometry, rain-contaminated measurements are more difficult to identify than the erroneous cross-track orientation in QuikSCAT wind retrievals (Weissman et al. 2002).

d. Sea-ice masking

Accurate wind velocities cannot be estimated from σ_0 measurements having significant ice in the antenna footprints. Coastal ice shelves and large icebergs can be detected using high-resolution scatterometer measurements of σ_0 and moderate-resolution brightness temperature measurements from multichannel microwave radiometers (see Remund and Long 2003 and references therein). For the present study, scatterometer measurements over sea ice were excluded from analysis based on conservative estimates of sea-ice edge extents calculated from SSM/I brightness temperatures. During each month, the locations of ice detections from all operating SSM/I instruments were accumulated on a 0.25° grid. At each longitude on the grid, the ice edge was defined as the equatorwardmost latitude containing at least one SSM/I sea-ice detection during the month and separated from the polar ice packs or land by less than 200 km. Large icebergs within 200 km of the continuous ice shelf or land thus extended the conservative ice edge equatorward, assuring that no contaminated scatterometer wind measurements were included in the comparison calculations in sections 4 and 5.

e. Cross-swath variations in wind measurement accuracy

Freilich and Dunbar (1999) showed that there is no evidence of significant variations in the accuracies of NSCAT wind speed and direction retrievals across either of the two parallel swaths. For QuikSCAT, however, the systematic cross-track variations in the azimuthal diversity of collocated σ_0 measurements results in cross-track variations in the accuracies of the wind vector estimates. For wind vector cell locations near the
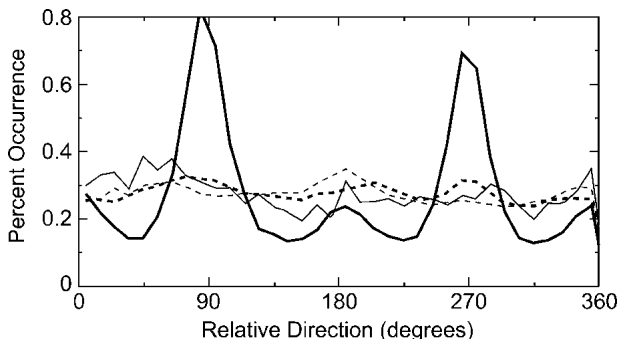

FIG. 5. Histograms of wind directions relative to the satellite subtrack from QuikSCAT wind retrievals (heavy solid and dashed lines) and buoy observations (thin solid and dashed lines) during raining conditions (solid lines) and nonraining conditions (dashed lines).

nadir track of the satellite, the relative azimuths of the measurements from the two fore looks are nearly the same, and differ by about 180° from the collocated measurements from the two aft looks. Near the outer edges of the swath, all of the collocated measurements have azimuth angles near 90° or 270° relative to the satellite subtrack.

The variation of QuikSCAT vector wind accuracy as a function of cross-swath location can be assessed from comparisons with NWP analyses of 10-m winds. Since the statistics of the wind velocity errors in the NWP wind fields do not vary with location within the QuikSCAT swath, any systematic cross-swath variations in low-order comparison statistics can be interpreted as swath-dependent errors in the scatterometer wind velocities. The operational ECMWF and NCEP analyses of 10-m winds (available every 6 h on a $1° \times 1°$ grid) were interpolated to the space–time locations of nonraining QuikSCAT measurements from 2 yr of global ocean data preceding the January 2002 initiation of assimilation of QuikSCAT data into the operational ECMWF and NCEP models. The magnitude of each interpolated wind vector was obtained by trilinear interpolation of the gridded NWP wind speeds, and the direction of the interpolated wind vector was obtained by the trilinear interpolation of the zonal u and meridional v components of the NWP gridded 10-m winds.

Feature mislocations in the NWP 10-m wind analyses and directional ambiguity removal errors in the scatterometer data can yield distributions of wind direction differences that are not well characterized by low-order statistical moments. Standard deviations of the QuikSCAT minus NWP wind speed and direction differences were therefore calculated only for cases where the QuikSCAT and interpolated NWP wind directions differed by less than 90°. It was assumed that larger discrepancies resulted from feature mislocations in the NWP wind analyses or gross directional ambiguity removal errors in the scatterometer processing. This screening procedure eliminated only 2% of the QuikSCAT-NWP collocations.

For cross-track distances between about 300 and 700 km on both sides of the swath center, the standard deviation (s.d.) of speed differences (top panel of Fig. 6) is nearly constant with a value of about 1.5 m s^{-1}. The QuikSCAT speeds are slightly noisier near the swath center where the fore-aft differences in azimuth angle approach 180°, although the maximum standard deviation at nadir remains less than 1.6 m s^{-1}. The standard deviations of speed differences increase rapidly at cross-track distances greater than 800 km, corresponding to the outer region of the swath that is sampled only by the outer, vertically polarized beam with a very narrow range of nearly cross-track azimuth angles.

The overall s.d. of directional differences between QuikSCAT and NWP winds are approximately 21°, with larger differences found near the center and
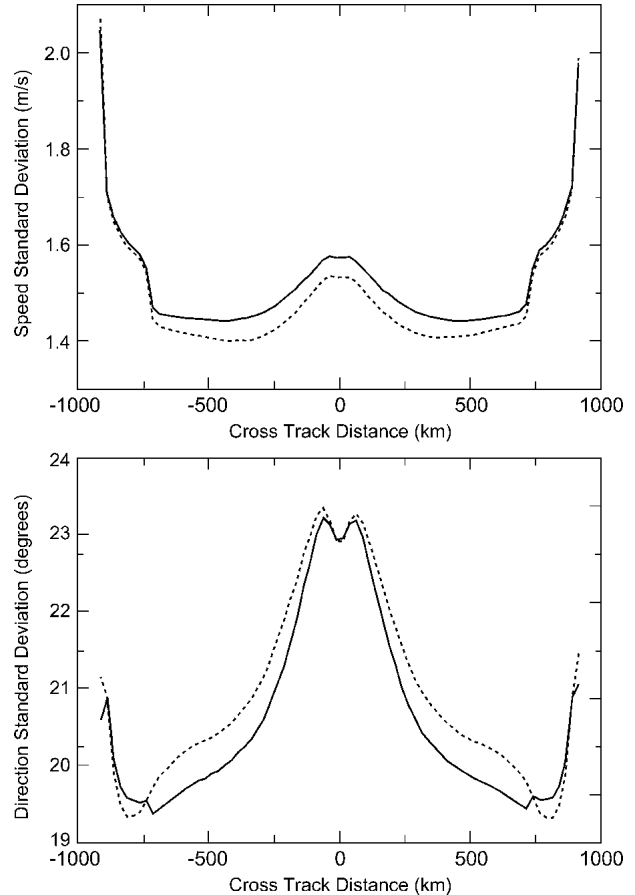

FIG. 6. Cross-swath variations in comparisons between QuikSCAT measurements and spatially and temporally interpolated ECMWF (solid lines) and NCEP (dashed lines) 10-m wind analyses: (top) standard deviations of wind speed differences, and (bottom) standard deviations of wind direction differences. Only collocated measurements for which QuikSCAT and NWP wind directions differed by less than 90° were considered (see text).

the outer edges of the swaths (bottom panel of Fig. 6). The total cross-swath variation in the rms directional difference s.d. is only about 5°.

It should be noted that the standard deviations of the wind speed and direction differences in Fig. 6 are not all attributable to errors in the QuikSCAT wind measurements. There are significant differences between QuikSCAT measurements and NWP estimates owing to errors in the NWP analyses and to the different spatial resolutions of about 25 km for the QuikSCAT measurements and about 500 km for the NWP analyses, despite a model grid resolution of less than 50 km (see the wavenumber spectra in Milliff et al. 2004).

Given the relatively constant speed and direction differences in Fig. 6 across most of the center 1600 km of the QuikSCAT measurement swath, the accuracies of the QuikSCAT vector wind estimates are assessed in section 2f from measurements within only this portion of the swath.

f. Buoy comparisons

Comparisons with collocated, simultaneous buoy measurements of wind adjusted for stability effects to obtain the 10-m equivalent neutral-stability wind provide the most accurate quantitative assessment of satellite wind measurement accuracy (see, e.g., Freilich and Dunbar 1999 and references therein for NSCAT, and Ebuchi et al. 2002 and Draper and Long 2002 for QuikSCAT). The results summarized here quantify the accuracy of the NSCAT and QuikSCAT data through comparisons with buoys that are representative of open-ocean winds measured by the scatterometer. Anemometer data were combined with measurements of air–sea temperature difference to calculate the equivalent neutral-stability winds at a height of 10 m above the sea surface from the buoy measurements using the method described by Liu and Tang (1996).

The full 9.5-month NSCAT dataset (September 1996–June 1997) and the first 2 yr of the QuikSCAT dataset (August 1999–July 2001) were used in the scatterometer–buoy comparisons presented here. Only the highest quality scatterometer and buoy data were considered. The objective criteria for selecting the open-ocean buoys and the data editing criteria are the same as those used by Freilich and Dunbar (1999). Briefly, the selected National Data Buoy Center (NDBC) buoys (Fig. 7 for QuikSCAT and Fig. 1 of Freilich and Dunbar for NSCAT) are all far enough from land to avoid spurious wind retrievals from side-lobe contamination of the scatterometer radar measurements and to minimize the effects of small-scale orographic wind features that can render buoy measurements at point lo-

cations unrepresentative of 25-km averaged scatterometer measurements. Collocations were defined to be scatterometer wind observations within 25 km and 30 min of buoy observations. As in the scatterometer–NWP wind comparisons in Fig. 6, the comparison statistics were further refined by eliminating scatterometer–buoy collocations with directions differing by more than 90°. This directional screening criterion resulted in elimination of 3.0% and 3.6% of the data for NSCAT and QuikSCAT, respectively. Based on the analysis in section 2e, the comparison statistics for QuikSCAT were computed from only the buoy collocations obtained in the middle 1600 km of the measurement swath. Finally, QuikSCAT measurements flagged for rain based on the MUDH algorithm described in section 2c were excluded. As no autonomous rain flagging capability is available for NSCAT, no explicit screening for rain contamination was performed on the NSCAT data.

Wind speed and direction comparisons between the midlatitude, open-ocean NDBC buoys and both NSCAT and QuikSCAT are summarized in Fig. 8. For equivalent neutral-stability 10-m wind speeds between about 3 and 18 m s^{-1}, the mean speed comparisons (top panel of Fig. 8) show that the biases relative to buoy wind speeds are only about −0.03 and 0.11 m s^{-1} for NSCAT and QuikSCAT, respectively. The overall rms speed differences are 1.3 m s^{-1} for NSCAT and 1.2 m s^{-1} for QuikSCAT. For buoy speeds exceeding about 18 m s^{-1}, QuikSCAT speeds are somewhat higher than NSCAT speeds, owing to changes in the QuikSCAT model function designed to address a small underestimate of
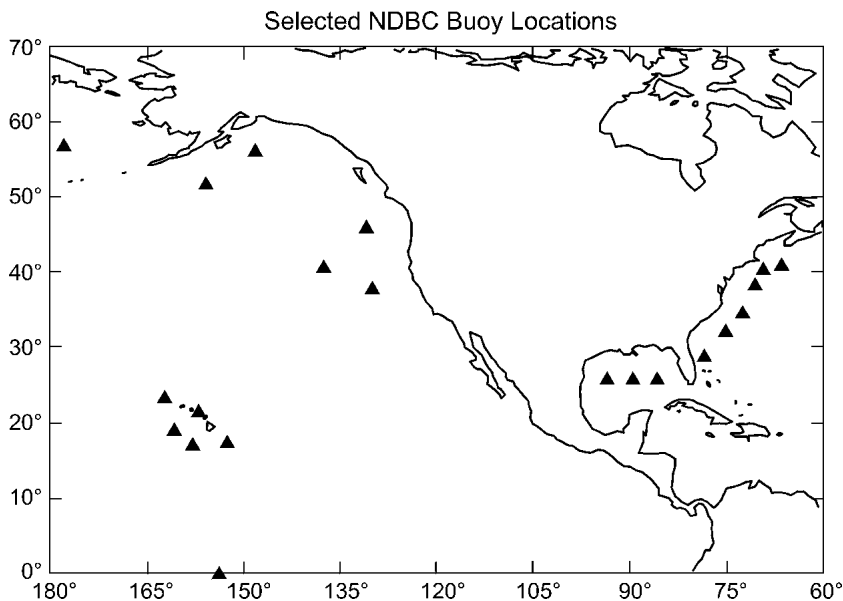

FIG. 7. Locations of the NDBC buoys used in the QuikSCAT analyses summarized in Figs. 8 and 16. See Fig. 1 of Freilich and Dunbar (1999) for the buoy locations used in the NSCAT analysis in Fig. 8 of the present study.
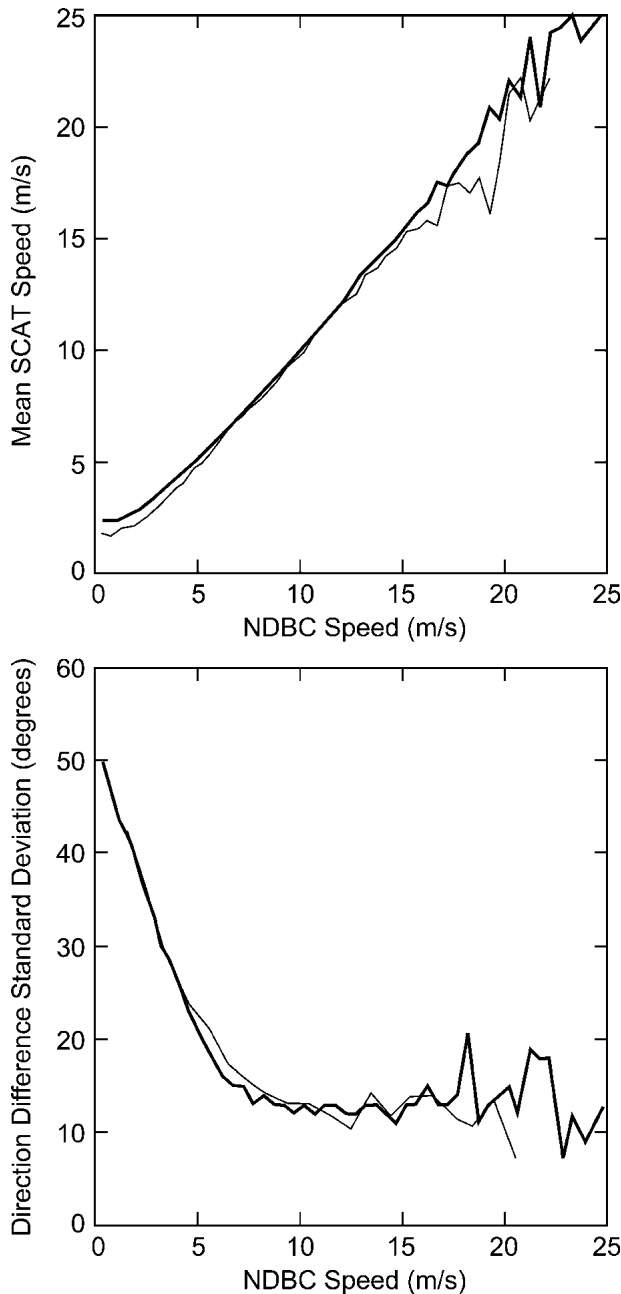
FIG. 8. NSCAT (thin lines) and QuikSCAT (heavy lines) wind speeds and directions compared with collocated buoy measurements: (top) conditional mean scatterometer speeds binned on buoy speed, and (bottom) standard deviations of buoy minus scatterometer wind direction differences as a function of buoy wind speed. Only collocated measurements for which the buoy and scatterometer directions differed by less than 90° were considered (see text). The noisiness at higher wind speeds is likely attributable to statistical uncertainties owing to the much smaller number of collocations at high wind speeds.

high wind speeds in the NSCAT data identified by Donnelly et al. (1999) and Yueh et al. (2000).

The standard deviations of directional differences are shown as a function of buoy wind speed in the

bottom panel of Fig. 8. The NSCAT and QuikSCAT curves are nearly identical for wind speeds below about 17 m s^{-1}.

The characteristic shapes of the curves in Fig. 8, with large directional difference s.d. at low wind speeds, rapidly decreasing to relatively constant values at wind speeds higher than about 6 m s^{-1} are consistent with the isotropic random component error model developed by Freilich (1997) and Freilich and Dunbar (1999). Assuming isotropic random component errors of 1 m s^{-1} for the buoy winds, fits to the observed wind speed bias as a function of buoy speed (top panel of Fig. 8) yield isotropic scatterometer random component error magnitudes of ~0.7 m s^{-1}. These errors are also consistent with the observed wind speed dependencies of the s.d. of differences between scatterometer and buoy wind speeds (not shown). Fits to the observed low-order directional difference statistics (bottom panel of Fig. 8) require larger isotropic scatterometer component error magnitudes of ~1.3 m s^{-1}.

Based on the different results obtained by these two approaches, B. A. Vanhoff and M. H. Freilich (2004, unpublished manuscript) have recently extended the isotropic random component error model of Freilich (1997) to include anisotropy. That analysis concludes that the QuikSCAT data have component error magnitudes of about 0.75 m s^{-1} in the along-wind direction and 1.5 m s^{-1} in the crosswind direction. The wind speed accuracy of QuikSCAT is thus approximately 1.7 m s^{-1} at all wind speeds. The wind direction accuracy is a sensitive function of wind speed at low wind speeds but improves rapidly with increasing wind speed. For a 6 m s^{-1} wind, the anisotropic component errors correspond to a directional accuracy of about 14°.

The larger errors in the crosswind component than in the along-wind component are likely an indication of larger errors in scatterometer estimates of wind direction than of wind speed. This could arise from σ_0 measurement errors or the nonlinear wind estimation process (Naderi et al. 1991). The σ_0 measurements depend more sensitively on wind speed than on wind direction. The use of multiple σ_0 measurements thus provides accurate estimates of wind speed (i.e., the along-wind magnitude) through cancellation of random errors. Conversely, directional information is extracted from differences in σ_0 measured from different viewing geometries. Random noise in the σ_0 measurements therefore does not cancel as in speed estimation. Since all of the directional ambiguities in a given scatterometer wind vector cell typically have similar speeds but vary widely in direction, ambiguity removal errors contribute principally to directional (rather than speed) errors.

Larger differences between scatterometer and buoy estimates of wind direction may also arise from actual differences between wind and stress directions. The direction of the surface stress vector is a function of wind–wave and swell directional distributions as well as

the wind direction (Geernaert et al. 1993; Rieder et al. 1994; Grachev et al. 2003). The stress direction measured by the scatterometer can therefore differ from the wind direction measured by buoys. This is especially the case at low wind speeds and in the vicinity of meteorological fronts.

For the above reasons, the errors are expected to be larger in scatterometer estimates of wind direction than of wind speed. To lowest order, the directional errors contribute principally to spurious cross-wind variability, thus resulting in larger errors in the cross-wind direction. For the purposes of the analyses in sections 4 and 5, the important point in the comparisons with buoy observations in Fig. 8 is that the NSCAT and QuikSCAT observations have nearly identical accuracies and that the scatterometer measurement accuracies are very similar to the accuracies of buoy measurements of near-surface winds.

3. Effects of atmospheric stability and surface ocean currents

The fact that scatterometers measure the surface wind stress has two important implications for interpretation of comparisons between NWP model winds and scatterometer observations. The first of these is that scatterometer winds are reported as the equivalent neutral-stability wind at a height of 10 m above the sea surface, as discussed in section 2a, while NWP analyses are intended to be estimates of the actual winds at 10 m. For determining air–sea fluxes of momentum, the scatterometer observations of equivalent neutral-stability wind are simply related to the wind stress through a neutral-stability drag coefficient. NWP analyses of 10-m winds must be adjusted for the effects of atmospheric stability to estimate the surface stress accurately, although this is seldom done in practice.

The second consideration is that scatterometers measure the actual stress imposed on the sea surface by the wind. This stress is determined by the vector difference between the wind and the surface ocean velocity at each measurement location. Scatterometers thus measure the wind relative to the moving sea surface. This is precisely the wind quantity that is appropriate for determination of air–sea fluxes of momentum, heat, and gases. In contrast, NWP analyses are estimates of the 10-m winds relative to fixed locations (the model grid points). In regions of strong currents, it has been shown that the surface ocean velocity can introduce differences of order 1 m s^{-1} between scatterometer and NWP winds (Cornillon and Park 2001; Kelly et al. 2001; Chelton et al. 2004). For accurate determination of air–sea fluxes, the 10-m winds from NWP models must therefore be adjusted for the effects of surface ocean currents (Pacanowski 1987). This also is not generally done in practice.

Accurate comparisons between collocated scatter-

ometer and NWP winds thus require adjustments of the NWP winds to account for the effects of atmospheric stability and surface ocean currents. These quantities are not available for every QuikSCAT–NWP collocation. Estimates of stability effects could be obtained from the NWP model analyses of air–sea temperature difference and surface humidity, but the uncertainties of these fields are large. Such corrections have not been implemented for the comparisons presented in sections 4 and 5. Corrections for ocean current effects are even more problematic since accurate estimates of the time-varying surface ocean currents are not available.

To the extent that the atmospheric boundary layer is near neutrally stable over most of the World Ocean, collocated scatterometer observations of equivalent neutral-stability winds at 10 m and NWP analyses of 10-m winds should be directly comparable in regions of weak surface ocean currents. At times and locations of significant deviation from neutral stability, the two will differ. Based on stability corrections calculated from global ocean buoy measurements, Mears et al. (2001) concluded that anemometer measurements of 10-m winds (which are the winds estimated by NWP models) are typically about 0.2 m s^{-1} lower than the equivalent neutral-stability winds at 10 m. This mean difference is verified in section 5 by the heavy solid and dashed lines in Fig. 16. The sign of this difference corresponds to the expected slightly unstable atmospheric boundary layer over most of the World Ocean.

4. Root-mean-squared component differences

The rms differences between the ECMWF analyses and scatterometer observations of u and v are shown, respectively, in the left and right panels of Fig. 9. During the 9.5-month NSCAT sampling period September 1996–June 1997, referred to here as "the 1997 time period" (top two panels), the rms differences in the relatively steady tradewind regimes of the Atlantic and Pacific and in the monsoon winds of the Arabian Sea were 1.5–2 m s^{-1} in both components. Elsewhere, the rms differences were larger, especially in u. Typical rms values of the u differences were more than 3 m s^{-1} at middle and high latitudes. The rms values of the v differences were somewhat smaller but still exceeded 2.5 m s^{-1} over much of the mid and high-latitude oceans. The bands of relatively large rms differences in both components just north of the equator in the Atlantic and Pacific are suggestive of ECMWF misplacement and underestimates of the winds in the intertropical convergence zone (ITCZ).

As discussed in section 3, the fact that the scatterometer winds are observations of equivalent neutral-stability winds at 10 m, while the NWP winds are the 10-m wind analyses without adjustments for atmospheric stability accounts for rms differences of about 0.2 m s^{-1} between the scatterometer and NWP winds.
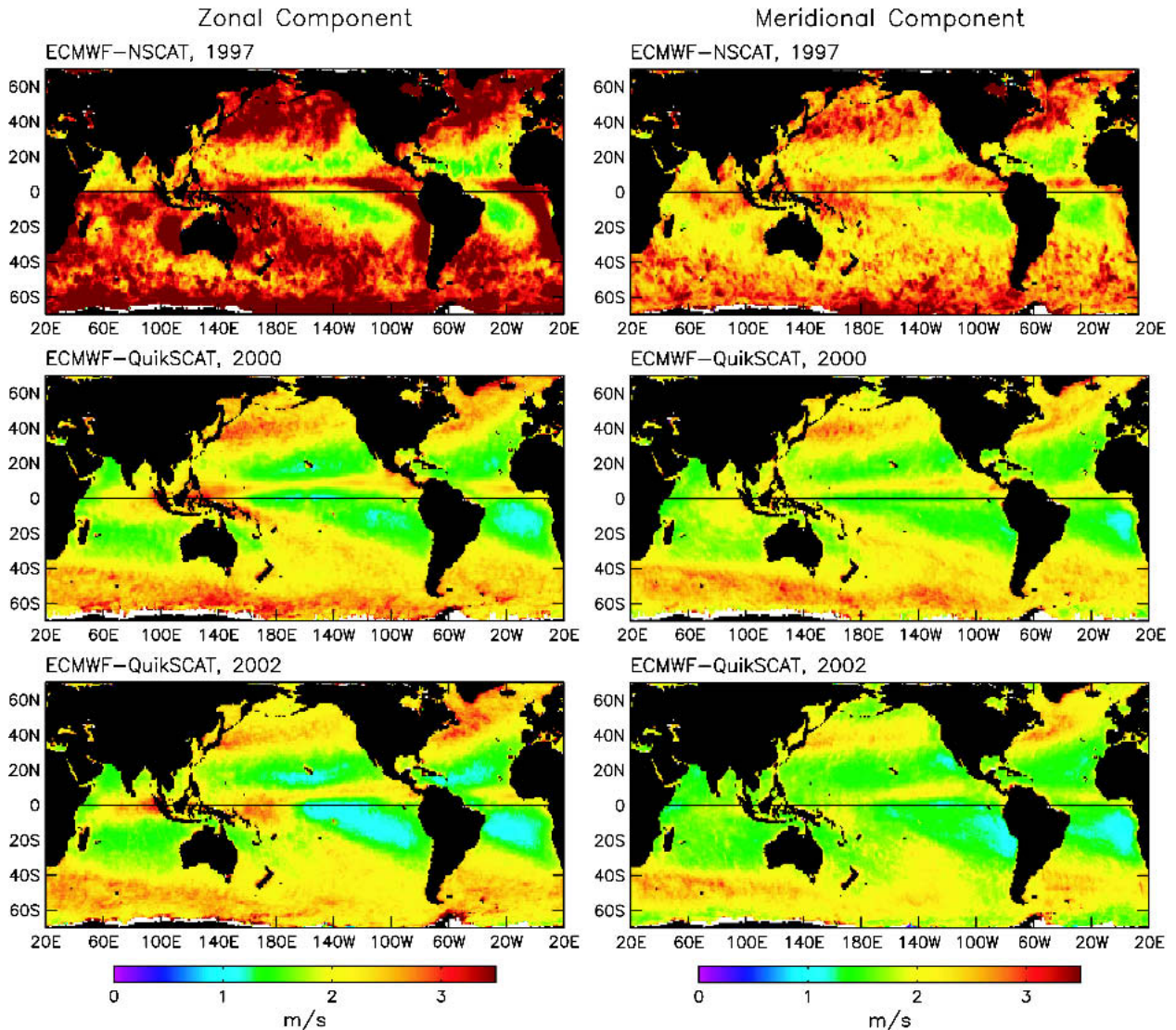
FIG. 9. The rms of (left) zonal component differences and (right) meridional component differences between ECMWF analyses of 10-m winds and scatterometer observations of equivalent neutral-stability winds at 10 m for the three time periods considered in this study. The "1997"period" [(top) (Sep 1996–Jun 1997)] corresponds to the NSCAT observational period, the "2000 time period" [(middle) (Aug 1999–Jul 2000)] corresponds to the first year of the QuikScat mission, and the "2002 time period [(bottom) (Feb 2002–Jan 2003)] corresponds to the first year of assimilation of QuikScat data into the ECMWF and NCEP models. The NWP gridded wind fields were interpolated to the time and location of each scatterometer observation as described in section 2e and the rms differences were computed from all of the collocations within each 1°-square region.

This is negligible compared with the magnitudes of the rms differences in Fig. 9. Based on buoy comparisons, the errors of the NSCAT winds are about 0.75 and 1.5 m s^{-1} for the along-wind and crosswind components, respectively (section 2f). Most of the rms differences during the 1997 time period can therefore be attributed to errors in the ECMWF analyses and differences resulting from the coarser spatial resolution of the ECMWF wind estimates.

The rms component differences between ECMWF analyses and QuikSCAT observations of 10-m winds for the 12-month period August 1999–July 2000, re-

ferred to here as "the 2000 time period," are shown in the middle panels of Fig. 9. The geographical patterns of the rms differences were generally similar to the patterns during 1997, but with much smaller magnitudes. This is especially true for u, for which the rms values decreased by nearly a factor of 2 to magnitudes about the same as the rms values of the v differences. The rms differences in each component were less than 1.5 m s^{-1} in the tradewind regimes, and were typically 2–2.5 m s^{-1} at middle and high latitudes and along the ITCZ. The changes in the ECMWF model that likely had the greatest impact on the accuracy improvement between

the 1997 and 2000 time periods are the implementation of 4D-VAR data assimilation on 25 November 1997 and an increase in the model grid resolution from T213 to T319 (i.e., from 0.845° to 0.564°) on 1 April 1998.

The interest here is primarily on the large scales. We note, however, that the rms component differences between ECMWF analyses and QuikSCAT observations of 10-m winds are locally large near many islands, especially in the Tropics. These larger rms differences are mostly attributable to wind shadows that are resolved by the QuikSCAT observations (Xie et al. 2001; Chavanne et al. 2002; Chelton et al. 2004; M. H. Freilich et al. 2004, unpublished manuscript) but are poorly represented by the NWP models.

The rms component differences for the first year after assimilation of QuikSCAT data into the ECMWF model (February 2002–January 2003, referred to here as "the 2002 time period") are shown in the bottom panels of Fig. 9. Though much smaller than the dramatic change between the 1997 and 2000 time periods, a further general improvement in the accuracy of the ECMWF analyses of 10-m winds is apparent. In addition to assimilation of QuikSCAT data, the improved accuracy during the 2002 time period may be attributable to the increase in the model grid resolution from T319 to T511 (i.e., from 0.564° to 0.352°) on 21 November 2000.

A notable characteristic of the comparisons between ECMWF and QuikSCAT data during the 2000 and 2002 time periods is the locally larger rms differences of both u and v in regions of strong currents: the Agulhas Return Current in the southwest Indian Ocean, the Antarctic Circumpolar Current in the South Pacific, the Gulf Stream in the North Atlantic, and the Kuroshio Extension in the North Pacific. This is attributable at least in part to the fact that scatterometers measure winds relative to a moving sea surface while NWP models estimate winds relative to fixed locations. The strong mean flow of these currents can generate differences of order 1 m s^{-1} between scatterometer and NWP or buoy winds. In the vicinity of the Pacific equatorial cold tongue, for example, Kelly et al. (2001) showed that the equatorial current system results in biases of more than 0.5 m s^{-1} between QuikSCAT winds and the winds measured by the Tropical Atmosphere–Ocean (TAO) moorings. Similarly, Chelton et al. (2004) showed that the surface current modifies the mean QuikSCAT winds by nearly 1 m s^{-1} over the core of the Gulf Stream.

The rms differences between NWP and QuikSCAT winds are also influenced by the surface velocity of energetic eddies associated with the strong currents. In the Gulf Stream region, for example, Cornillon and Park (2001) showed that eddies generate relatively small-scale variations of order 1 m s^{-1} in the QuikSCAT winds.

The major ocean currents are associated with sea-surface temperature (SST) fronts that also contribute to the larger rms component differences between the NWP and QuikSCAT winds. These SST fronts exert a strong influence on the stability of the marine atmospheric boundary layer. The low-level wind field is significantly altered through stability effects on vertical turbulent mixing and deepening of the atmospheric boundary layer (Xie 2004; Chelton et al. 2004). These SST-induced spatial variations in the near-surface winds near major ocean currents are underrepresented in the NWP models (Chelton et al. 2004; Chelton 2005), thus resulting in increased rms differences between the NWP and QuikSCAT winds.

The evolution of the accuracies of the NCEP analyses of 10-m winds can similarly be assessed from rms component differences. During the 1997 time period, NCEP (then called the National Meteorological Center) did not produce 10-m wind analyses. For the purposes of this study, the winds at 10 m were estimated by reducing the 1000-mb wind analyses by a multiplicative scaling factor of 0.84 with no rotation.[3] Although crude, these adjustments provide an approximate measure of the accuracies of NCEP analyses during the time period of the NSCAT mission. The NCEP 1000-mb wind analyses during the 1997 time period were available at 6-h intervals on a 2.5° × 2.5° grid. The scaled and rotated 1000-mb winds were trilinearly interpolated in space and time to each NSCAT observation point by the same method applied above for the ECMWF collocations.

It was not necessary to convert 1000-mb winds to 10-m winds for the 2000 or 2002 time period since 10-m wind fields were available from NCEP. The NCEP 6-hourly, 1° × 1° gridded analyses of 10-m winds were collocated to the QuikSCAT observation times and locations by trilinear interpolation.

The geographical patterns of the rms values of the u and v differences for NCEP (Fig. 10) are very similar to those for ECMWF. In particular, the rms differences were much larger during the 1997 time period and the largest magnitudes occurred in the same regions for both NCEP and ECMWF. Over the midlatitude South Indian Ocean, the rms differences of v were somewhat larger for NCEP than for ECMWF during the 1997 and 2000 time periods. During the more recent 2002 time period, however, the rms differences of both u and v over the midlatitude South Indian Ocean were slightly smaller for NCEP. In the steady tradewind regions of the Atlantic and Pacific, the rms differences in both u

---

[3] The 0.84 scaling factor and 0° rotation to estimate 10-m winds from NCEP 1000-mb winds were determined empirically from global, collocated NCEP 1000-mb winds and NSCAT 10-m winds based on examination of histograms of the wind speeds (see, e.g., Freilich and Dunbar 1993) and wind direction differences. From sensitivity studies, we determined that the conclusions presented here change only qualitatively for values of the scaling factor ranging from 0.8 to 0.9, which spans the range of previously published values of the relationship between the winds at 1000 mb and 10 m (Freilich and Dunbar 1993; Reynolds et al. 1989).
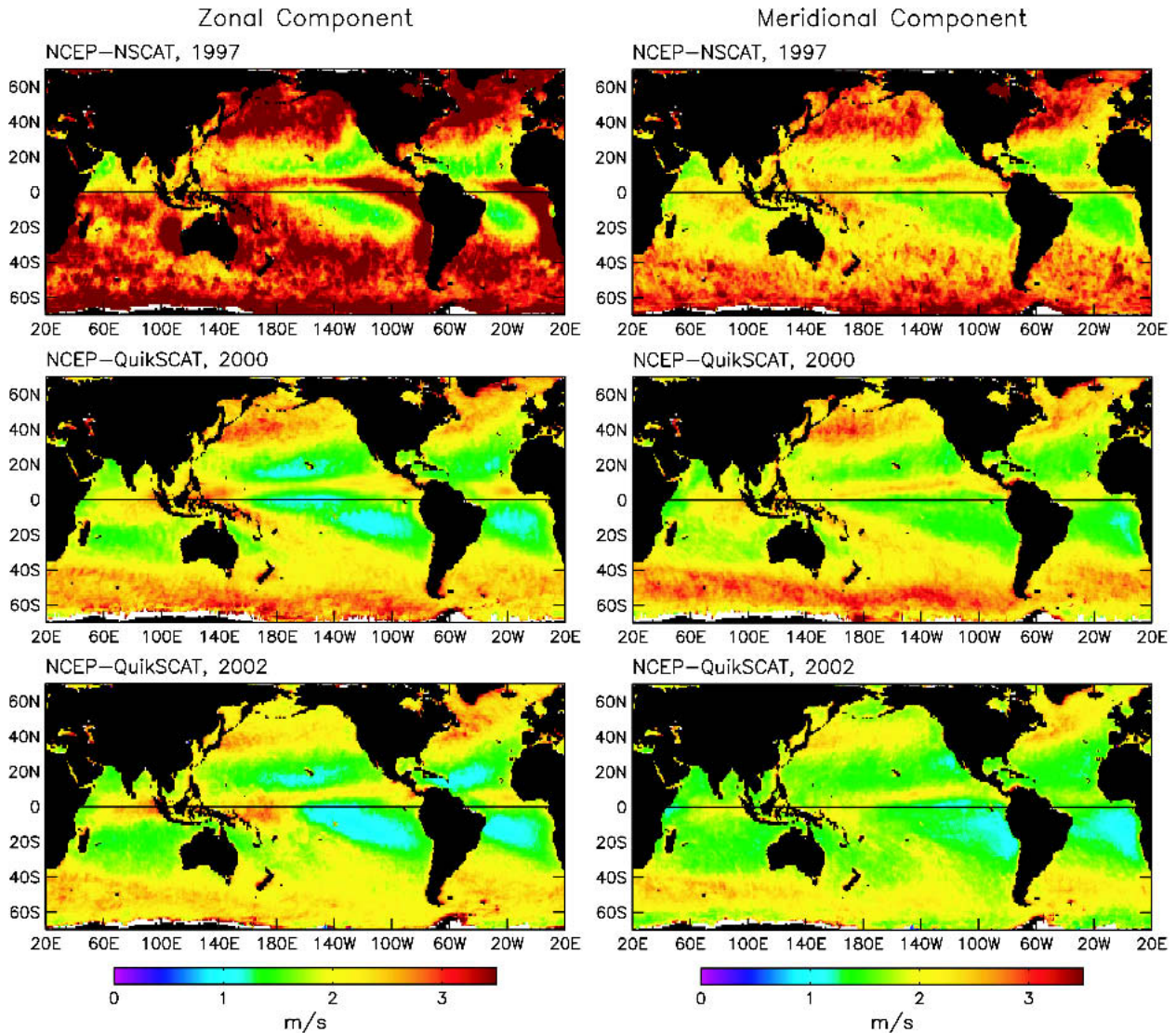
FIG. 10. The same as Fig. 9, except the rms of zonal and meridional component differences between NCEP analyses of 10-m winds and scatterometer observations of equivalent neutral-stability winds at 10-m winds. For the 1997 time period, the NCEP winds at 1000 mb were converted to 10-m winds as discussed in the text. The top panels should therefore be interpreted with caution since the results are somewhat sensitive to the choice of the scaling factor for estimating 10-m winds from the NCEP analyses of 1000-mb winds available for this time period.

and v were likewise slightly smaller for NCEP during 2002. In all of these regions of relatively steady winds, the larger rms values of the component differences in the ECMWF fields are at least partly attributable to an apparent bias of about -0.4 m s^{-1} in the ECMWF wind speeds (see section 5). The effects of this bias are less evident in regions of lower directional steadiness.

The improvements in the NWP wind fields are summarized in the top four panels of Fig. 11 from histograms of the rms values of the component differences. The dynamic ranges and the modes of the histograms of rms values of the u differences decreased significantly from 1997 to 2000 for both NWP models. From 2000 to 2002, the mode of the distribution of the rms values of

the u differences decreased only slightly for ECMWF but more significantly for NCEP. For the v differences, the modes of the distributions for both ECMWF and NCEP decreased significantly between each of the three successive time periods considered here.

Maps of the rms values of the wind component differences between the two NWP models collocated to the scatterometer observations are shown in Fig. 12. The geographical patterns of the rms differences between the NWP models are very similar to those of the rms differences between the NWP and scatterometer winds in Figs. 9 and 10. During the 1997 time period, the rms differences between ECMWF and NCEP were about 1 m s^{-1} in the tradewind regimes and about
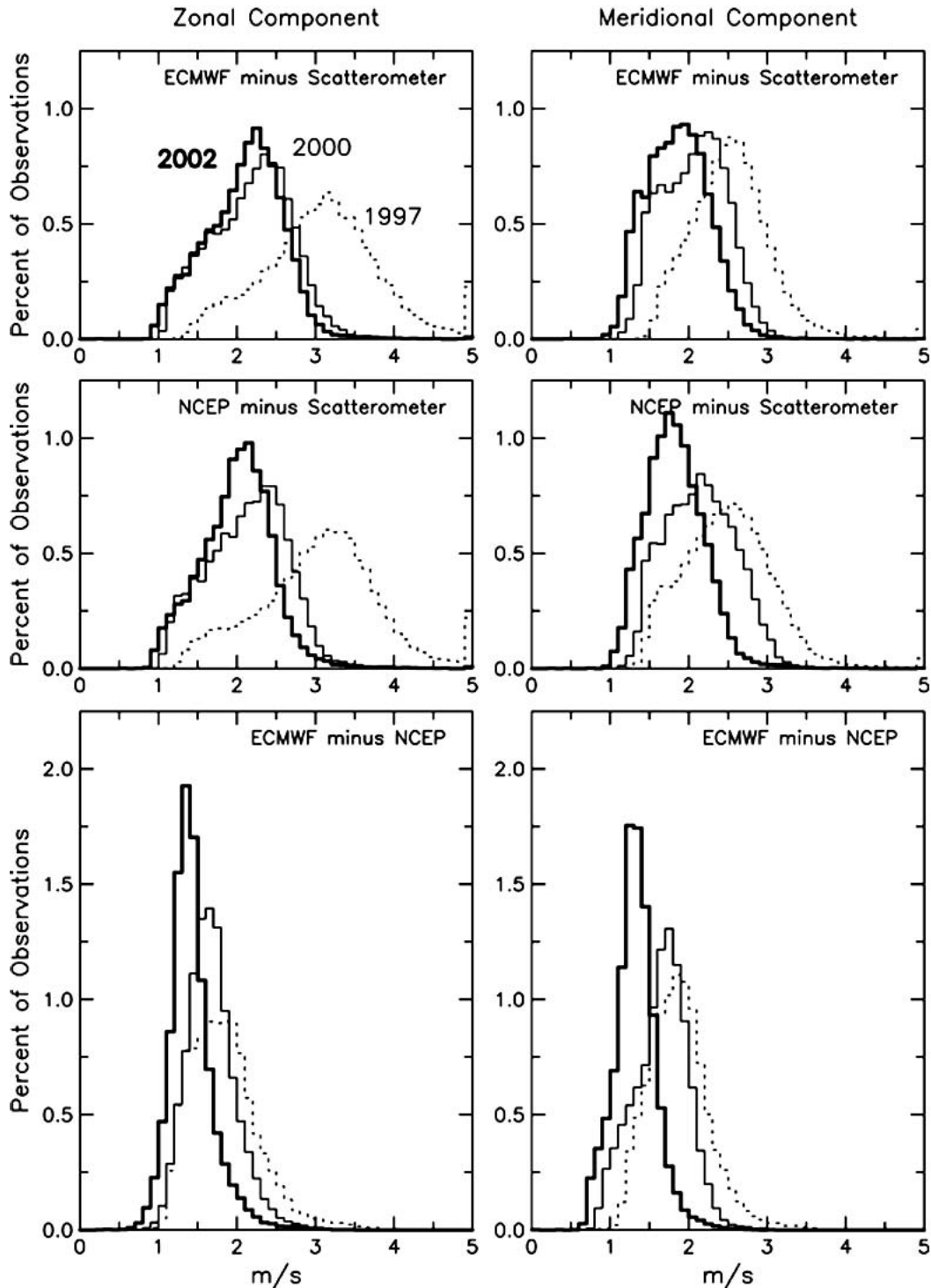
FIG. 11. Histograms of the rms of the wind component differences between the NWP analyses of 10-m winds and scatterometer observation of equivalent neutral-stability winds at 10 m for the 1997 (dotted lines), 2000 (thin solid lines), and 2002 (thick solid lines) time periods. The rms differences for the (left) zonal and (right) meridional components. The three pairs of histograms of the rms of component differences are (top) scattereometer vs ECMWF from Fig. 9 , (middle) scatterometer vs NCEP from Fig. 10 , and (bottom) ECMWF vs NCEP from Fig. 12 .
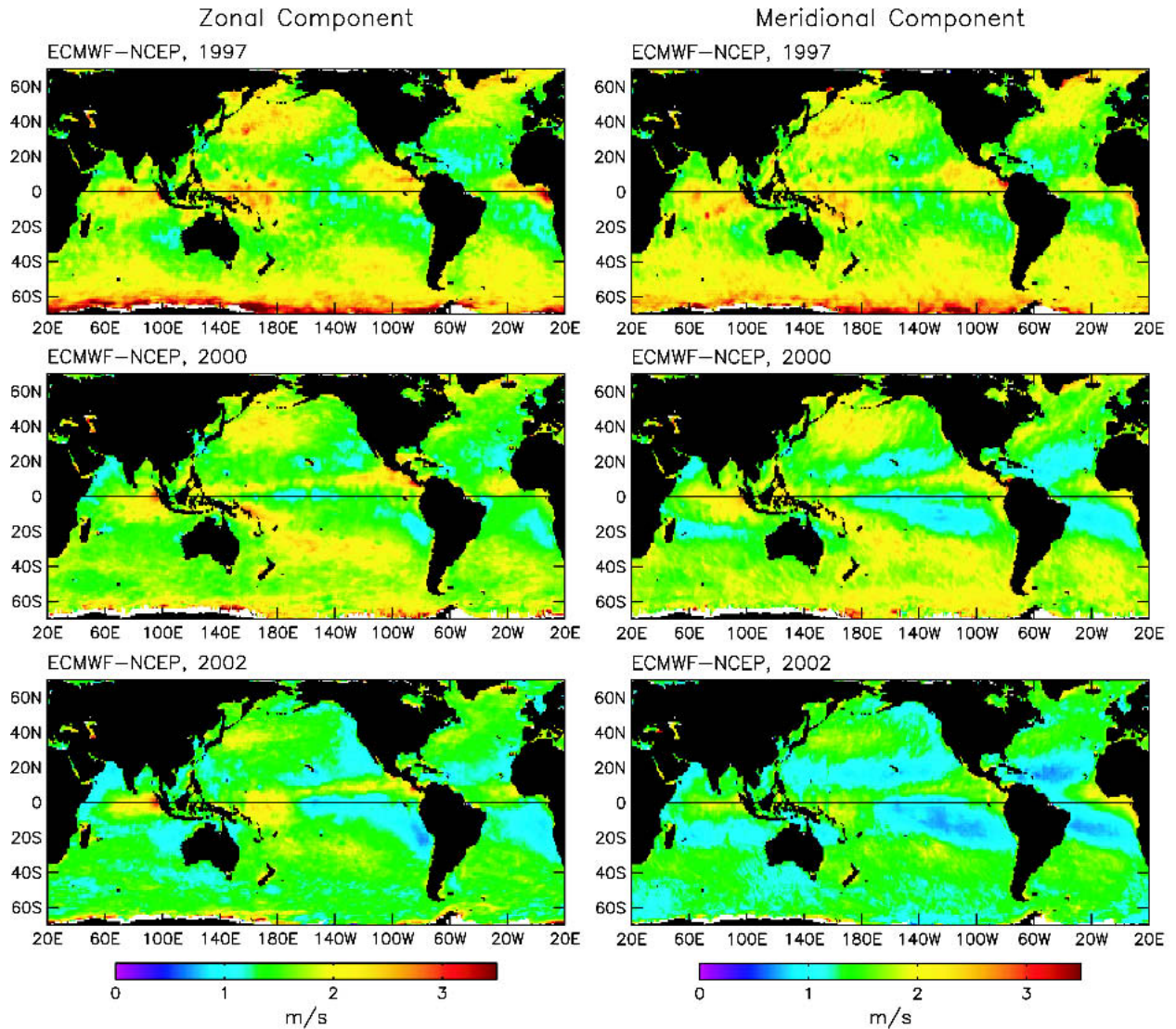
FIG. 12. The same as Figs. 9 and 10, except the rms of zonal and meridional component differences between ECMWF and NCEP analyses of 10-m winds.

2 m s^{-1} in the midlatitude westerly regimes. The rms differences increased to more than 3 m s^{-1} at high southern latitudes. The large rms differences at high southern latitudes during the 1997 time period were essentially eliminated in the 2000 time period and the magnitudes of the rms differences decreased by a few tenths of a meter per second in each component over most of the World Ocean. The magnitudes of the rms differences decreased by somewhat more in 2002, during which the rms values exceeded 1.5 m s^{-1} in only a few limited regions.

The evolutionary improvements in the agreement between the two NWP models are summarized by the histograms of the rms values of the component differences in the bottom pair of panels in Fig. 11. The dy-

namic ranges of the differences decreased significantly between each of the three time periods considered here. For the 2002 time period, 80% and 87% of the rms values of the u and v differences, respectively, fell within the narrow range between 0.75 and 1.5 m s^{-1}.

The rms differences in Figs. 9–12 thus indicate that the 10-m wind analyses from the ECMWF and NCEP models appear to be converging, with closer agreement model-to-model than between either model and reality, as represented here by the scatterometer data. In part, this is due to the fact that, while the model grid resolutions are less than 50 km, the feature resolution in the 10-m winds from both NWP models is only about 500 km (Milliff et al. 2004), whereas the scatterometer winds have a much higher resolution of 25 km. Perhaps

more importantly, the accuracies of the two operational NWP models are limited by assimilation of essentially the same in situ and satellite sounding data.

5. Mean wind speed differences

A subtle feature of the differences between the NWP and scatterometer winds that is not clearly apparent from the rms component differences examined in section 4 is the existence of an apparent bias in the wind speeds in ECMWF analyses of 10-m winds. This is shown in Figs. 13 and 14 from global maps and histograms of the mean speed differences for each of the three time periods considered in this study. While there were localized regions of both positive and negative mean speed differences between ECMWF and NSCAT in excess of 1 m s^{-1} during the 1997 time period (top panel in the left column of Fig. 13), the overall global mean difference was only -0.03 m s^{-1}. During the 2000 and 2002 time periods, however, ECMWF wind speeds were lower than QuikSCAT wind speeds throughout most of the World Ocean (bottom two panels in the left column of Fig. 13). Globally, the mean ECMWF minus QuikSCAT wind speed differences during the 2000 and 2002 time periods were -0.61 and -0.63 m s^{-1}, respectively. Because of the ocean current effects discussed below, these biases increase to -0.74 and -0.71 m s^{-1} when the region south of 40S is excluded from the average. As shown by the solid circles in Fig. 15, these biases decreased somewhat with increasing wind speed.

Close inspection of the bottom two panels in the left column of Fig. 13 reveals regions of locally reduced relative bias between ECMWF and QuikSCAT mean wind speeds. Examples include the equatorial cold tongues in the Pacific and Atlantic and the cold water on the inshore side of the Gulf Stream. The mean near-surface wind speeds are lower in these regions because of increased stabilization of the marine atmospheric boundary layer over the cold water (Xie 2004; Chelton et al. 2004). The zonal bands of locally increased relative bias between ECMWF and QuikSCAT wind speeds just north of the equatorial cold tongues and seaward of the Gulf Stream are regions where the low-level winds are accelerated in association with destabilization of the boundary layer over the warmer water, resulting in higher mean wind speeds. Underrepresentation of these SST-induced modifications of low-level winds in the NWP models (Chelton et al. 2004; Chelton 2005) results in geographical variations from the global mean relative bias of about -0.6 m s^{-1} between ECMWF and QuikSCAT wind speeds.

A prominent feature in the 2000 and 2002 comparisons between ECMWF and QuikSCAT wind speeds is the surprising small-scale structure in the relative bias in the southwest Indian Ocean. There is an abrupt change from a bias of about -0.75 m s^{-1} north of about 40°S to near zero to the south. These two distinct re-

gimes are separated by a well-defined narrow and undulating line that coincides with the location of persistent meanders in the SST front associated with the Agulhas Return Current. Along this SST front, the geographical variations of the mean wind speed difference are mostly attributable to modulation of the low-level winds by SST-induced spatial variability in the stability of the atmospheric boundary layer. O'Neill et al. (2003; O'Neill et al. 2004, manuscript submitted to *J. Climate*) have shown that the scatterometer wind speeds over the persistent cold northward meanders of the SST front are 0.5–1.0 m s^{-1} lower than the wind speeds over the warmer water to the north. This effect, which is restricted to the immediate vicinity of the strong SST front, is underrepresented in the ECMWF winds, thus accounting for the undulating line that separates the two wind speed bias regimes.

To the south of the Agulhas SST front, the broad area of reduced relative bias during 2000 and 2002 is a region where the mean eastward winds blow parallel to the mean eastward surface velocity of the Agulhas Return Current and Antarctic Circumpolar Current (ACC). Because the mean surface velocity of the ACC is about 0.5 m s^{-1} in this region (O'Neill et al. 2004, manuscript submitted to *J. Climate*), the winds measured by a scatterometer are reduced by this amount, thus reducing the relative bias between QuikSCAT and ECMWF wind speeds. The QuikSCAT wind speeds are reduced by a similar amount over the ACC throughout the Southern Ocean, essentially eliminating the relative bias between ECMWF and QuikSCAT wind speeds that exists in lower latitude regions where the weaker surface ocean currents have less affect on the mean QuikSCAT winds.

It is challenging to quantify the partitioning of the global average relative bias of -0.6 m s^{-1} between errors in ECMWF and errors in QuikSCAT. The comparisons of ECMWF and QuikSCAT wind speeds with NCEP wind speeds in the middle and right columns of Fig. 13 and in the bottom two panels of Fig. 14 suggest that most of the relative bias is attributable to ECMWF; the overall global average NCEP minus QuikSCAT wind speed differences during the 2000 and 2002 time periods were -0.20 and -0.15 m s^{-1}, respectively. As discussed in section 3, biases of these magnitudes can be accounted for by the differences between the 10-m winds in the NWP analyses and the equivalent neutral-stability 10-m winds observed by QuikSCAT. The overall global average ECMWF minus NCEP wind speed differences during the 2000 and 2002 time periods were -0.41 and -0.48 m s^{-1}, respectively—that is, smaller than the mean speed difference between ECMWF and QuikSCAT by about the same amounts as the mean speed differences between NCEP and QuikSCAT.

The negative bias of about -0.4 m s^{-1} in the NCEP wind speeds over the ACC in the bottom two panels in the middle column of Fig. 13 is attributable to the
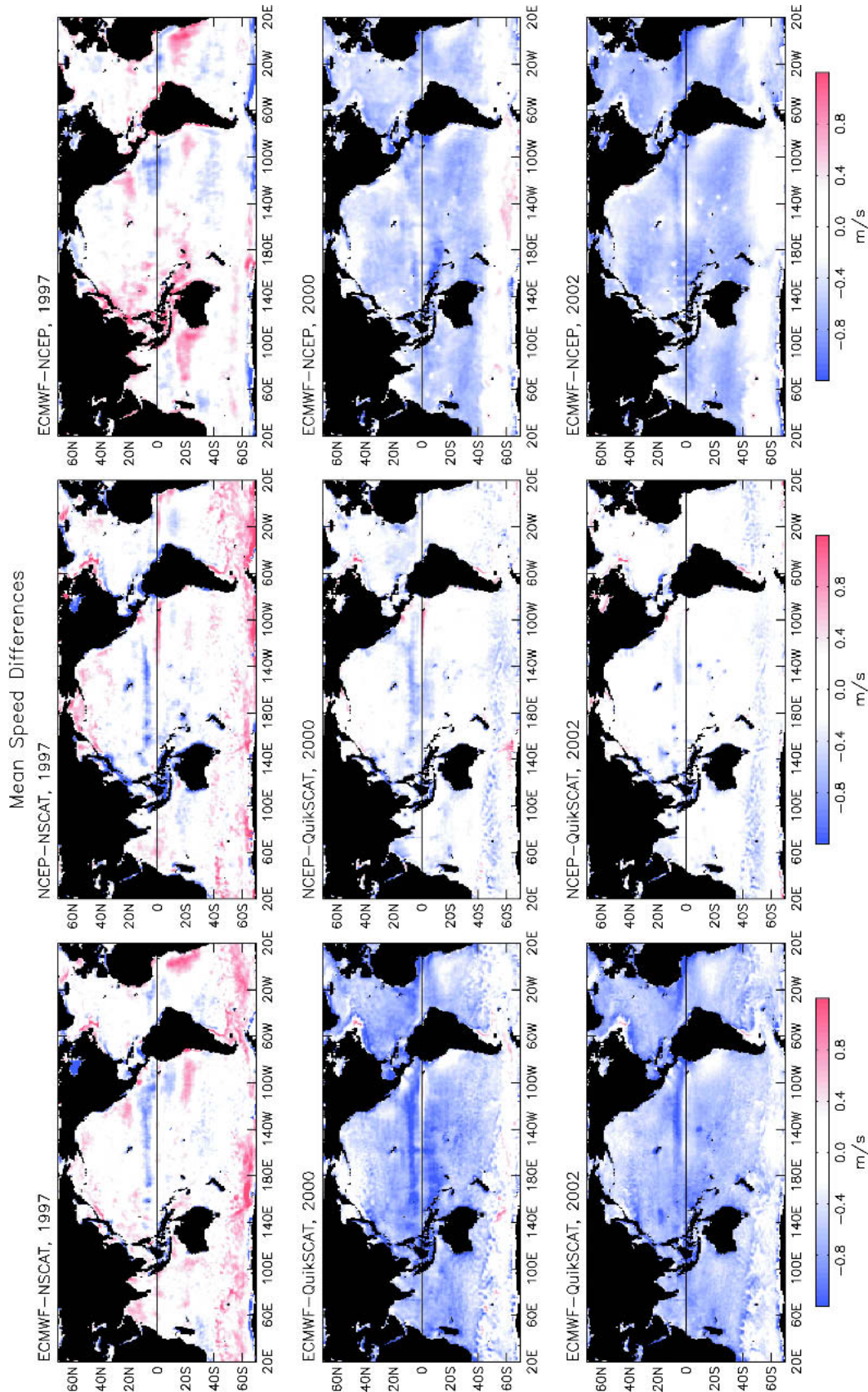
FIG. 13. The mean speed differences between scatterometer observations of equivalent neutral-stability winds at 10 m and ECMWF and NCEP analyses of 10-m winds for the three time periods considered in this study. The mean speed differences were computed from all of the collocated NWP and scatterometer winds within each 1°-square region. As in Fig. 10, the mean speed differences from NCEP during the 1997 time period in the top-middle and top-right panels should be interpreted with caution since the results are somewhat sensitive to the choice of the scaling factor for estimating 10-m winds from the NCEP analyses of 1000-mb winds available for this time period.
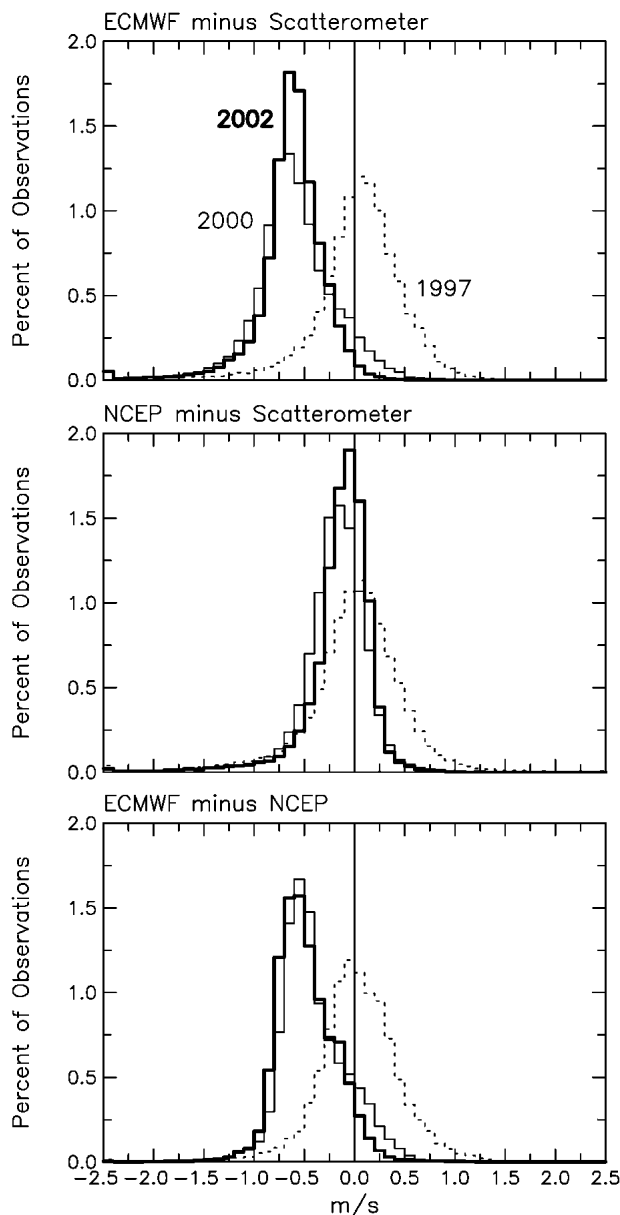
FIG. 14. Histograms of the mean wind speed differences between scatterometer observations of equivalent neutral-stability winds at 10 m and ECMWF and NCEP analyses of 10-m winds for the 1997 (dotted lines), 2000 (thin solid lines) and 2002 (thick solid lines) time periods. The histograms were computed from the mean wind speed differences in Fig. 13. Mean speed differences between the scatterometer observations and (top) ECMWF and (middle) NCEP; (bottom) mean speed differences between NCEP and ECMWF.

above-mentioned effects of surface ocean velocity on the comparisons between NCEP and QuikSCAT wind speeds. Elsewhere the relative bias between NCEP and QuikSCAT is near zero throughout the extratropical regions. As a consequence of this localized bias in the NCEP wind speeds, the relative bias between NCEP

and ECMWF is near zero over the ACC (bottom two panels in the right column of Fig. 13).

Except in the region of the ACC, the maps and histograms in Figs. 13 and 14 thus suggest that about -0.2 m s^{-1} of the approximate -0.6 m s^{-1} relative bias between ECMWF and QuikSCAT during the 2000 and 2002 time periods is attributable to the differences between the winds at 10 m and the equivalent neutral-stability winds at 10 m. The approximate -0.2 m s^{-1} global mean difference between ECMWF 10-m winds and equivalent neutral stability winds has been independently confirmed by H. Hersbach (2003, personal communication) from an analysis of stability effects on the 10-m winds in the ECMWF model. The remaining mean wind speed difference of about -0.4 m s^{-1} appears to represent a low bias in the ECMWF wind speeds during the 2000 and 2002 time periods.

The apparent bias of the ECMWF wind speeds was further investigated from comparisons with direct measurements by the 22 open-ocean NDBC buoys shown in Fig. 7. Time series of running 12-month average biases of ECMWF 10-m wind speeds and 10-m equivalent neutral stability wind speeds are shown in Fig. 16 by the heavy solid and dashed lines, respectively, for the 9-yr time period 1994–2002. The approximate constant offset of about 0.2 m s^{-1} between these two curves represents the average effects of stratification noted previously in section 3. The relative bias of the ECMWF wind speeds was coincidentally smallest during the first few months of the NSCAT mission; minimum biases of about -0.2 and 0 m s^{-1} occurred throughout the second half of 1996 for the 10-m winds and 10-m equivalent neutral stability winds, respectively. Maximum biases of about -0.6 and -0.4 m s^{-1} occurred in mid 1999, just prior to the July 1999 start of the QuikSCAT data record. The biases steadily decreased to local minima of about -0.45 and -0.25 m s^{-1} at the end of 2001. The biases of the ECMWF 10-m wind speeds deduced from this particular collection of 22 buoys are slightly smaller than the estimates deduced globally from Figs. 13–15.

For comparison, a time series of the running 12-month average bias of QuikSCAT 10-m equivalent neutral stability wind speeds collocated to the 22 open-ocean NDBC buoys is shown by the thin solid line in Fig. 16. Relative to this collection of buoys, the QuikSCAT wind speeds were biased high by about 0.15 m s^{-1} at the beginning of the data record. This bias remained relatively constant until the end of 2001, and then steadily decreased to near zero at the end of 2002. These biases are consistent with the overall average bias of 0.11 m s^{-1} deduced from the QuikSCAT–buoy comparisons in section 2f.

Although it is admittedly a challenge to eliminate small systematic errors in any wind estimates, the apparent global bias of about -0.4 m s^{-1} in the ECMWF 10-m equivalent neutral stability winds is significant for oceanographic applications. A bias of this magnitude is 6% of the typical open-ocean wind speed of about
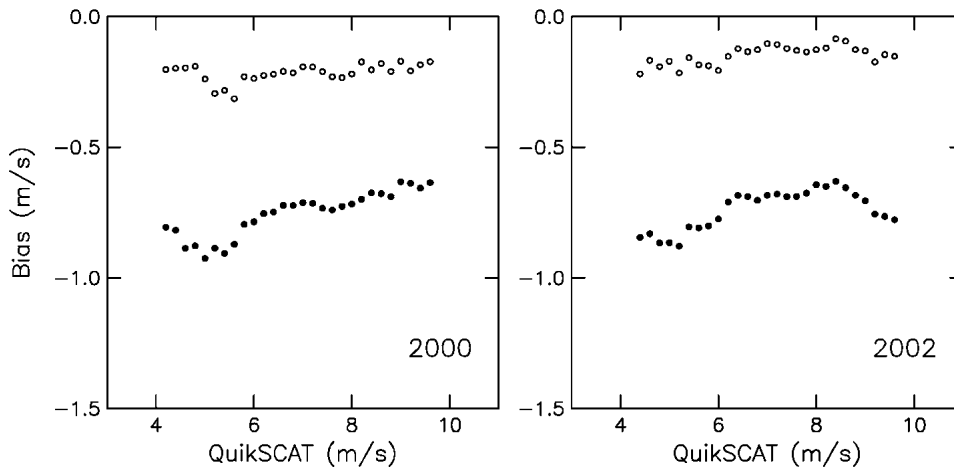
FIG. 15. Binned averages of the differences between QuikSCAT equivalent neutral stability 10-m wind speeds and the 10-m winds speeds from ECMWF (solid circles) and NCEP (open circles) as functions of the QuikSCAT wind speed for (left) 2000 and (right) 2002 for the latitude range from 40°S to 60°N.

7 m s^{-1}. Because the wind stress is related to the square of the wind speed, a 6% bias in the wind speed represents a bias of about 12% in the wind stress magnitude. Wind stress errors this large would result in significant errors in ocean general circulation models (OGCM). The poleward transports of western boundary currents, for example, could be underestimated by about 12% if an OGCM is forced by ECMWF winds.[4] If wind stress fields were constructed from the ECMWF 10-m wind analyses assuming a neutral-stability drag coefficient (that is, neglecting the effects of stratification), as is usually done, then the systematic error of the wind stress would include the effects of the full relative bias of about -0.6 m s^{-1} of the ECMWF 10-m winds. This would result in wind stresses biased lower than QuikSCAT stresses by nearly 20%, with a corresponding ~20% underestimate of the poleward transports of the western boundary currents.

6. Conclusions

The availability of high-quality scatterometer data from NSCAT during the 9.5-month period September 1996–June 1997 and from QuikSCAT since July 1999 provides an opportunity to investigate the recent evolution of the accuracy of 10-m wind analyses from operational NWP models. Detailed comparisons with buoy observations in section 2f concluded that the wind speed and direction accuracies are essentially the same

for NSCAT and QuikSCAT. The scatterometer measurement errors are best characterized in terms of random component errors, which are estimated to be about 0.75 and 1.5 m s^{-1} for the along-wind and cross-wind components, respectively. Scatterometer winds represent the equivalent neutral-stability winds at 10 m, which are typically about 0.2 m s^{-1} higher than the winds at 10 m because of the slightly unstable atmospheric boundary layer over most of the World Ocean.

The NSCAT and QuikSCAT winds were compared with collocated 10-m wind analyses from the ECMWF and NCEP models in sections 4 and 5. The rms differences between NWP analyses and scatterometer observations of 10-m wind components presented in section 4 indicate substantial improvements in the accuracies of both models over the 2-yr period from the end of the NSCAT data record in June 1997 to the beginning of the QuikSCAT data record in July 1999. Although modest in comparison, there were further improvements in the accuracies of the ECMWF and NCEP models between the first year of the QuikSCAT mission and February 2002 after both models began assimilating QuikSCAT data.

The reasons for the improvements of the ECMWF and NCEP 10-m wind analyses cannot be determined from the analysis presented here. Numerous changes were made to both models over the 6-yr time period, some of which were identified in section 4. Isolating the specific changes responsible for the improvements in the model accuracies is beyond the scope of this study, requiring more refined analyses than the bulk statistics presented in sections 4 and 5. The important conclusion from the results presented here is that rms differences between contemporary NWP winds and QuikSCAT winds during the most recent time period considered in this study (February 2002–January 2003) were about 2.0–2.5 m s^{-1} in both orthogonal components through-

---

[4] The "accumulated forecast stress" fields archived at ECMWF are unbiased relative to QuikSCAT wind stress fields (Chelton 2005). OGCMs forced by these forecast stress fields will therefore be immune to the bias of wind stress fields constructed from the 10-m wind fields based on one of the usual wind speed dependent formulations of the drag coefficient (e.g., Trenberth et al. 1990; Smith 1988).
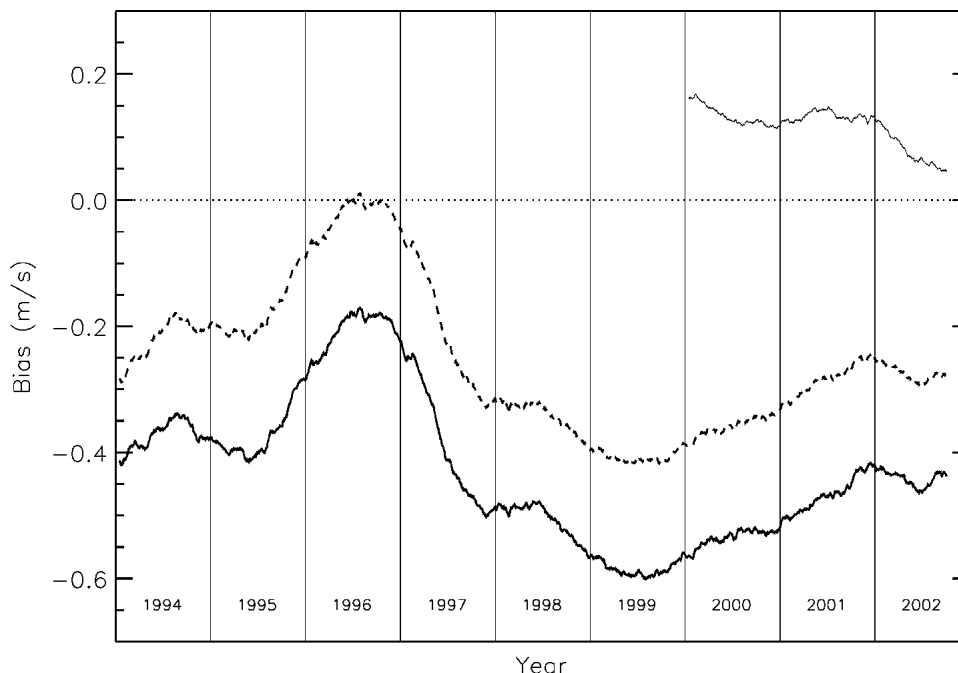
FIG. 16. Twelve-month running averages of wind speed biases relative to the collocated 10-m equivalent neutral stability wind speed measured by the 22 NDBC buoys shown in Fig. 7. Heavy solid line: ECMWF 10-m wind speeds. Heavy dashed line: ECMWF 10-m equivalent neutral stability winds speeds obtained from the ECMWF 10-m winds corrected using buoy measurements of air–sea temperature difference. Thin solid line: QuikSCAT equivalent 10-m neutral stability wind speeds.

out most of the World Ocean, decreasing to about 1.0–1.5 m s^{-1} in the tradewind regimes. By comparison, the rms component differences were 50%–100% larger during the September 1996–June 1997 time period of the NSCAT mission.

Because of the directional steadiness of the trade winds, most of the variability in these regions is in the along-wind component. Since the random errors of the QuikSCAT winds are estimated to be about 0.75 m s^{-1} in the along-wind direction, the rms component differences of 1.0–1.5 m s^{-1} between the NWP and QuikSCAT winds in the trade winds during the 2002 time period are approximately equally partitioned between errors in QuikSCAT and errors in the NWP winds. Outside of the trade winds, where the NWP–QuikSCAT rms component differences generally exceed 2.0 m s^{-1}, errors in the NWP winds are larger than errors in QuikSCAT winds.

A noteworthy feature of the comparisons between NWP and QuikSCAT winds is the slightly larger rms component differences of about 2.5–3.0 m s^{-1} over the major ocean currents, compared with about 2 m s^{-1} over the surrounding waters. These regional differences are at least partly attributable to the fact that scatterometers measure the winds relative to a moving sea surface while the NWP models estimate winds relative to fixed locations (the model grid points). The winds measured by a scatterometer are the winds that are

relevant to air–sea fluxes of momentum, heat and gases. For oceanographic applications, the effects of ocean currents on scatterometer winds should therefore not be considered a source of error in the scatterometer wind retrievals. To the contrary, scatterometry is the only source of wind information that provides the relative wind that is required for accurate determination of air–sea fluxes.

The larger rms differences between NWP and QuikSCAT winds near major ocean currents are also partly attributable to the influence of the associated SST fronts on the low-level wind field through SST modification of the stability of the atmospheric boundary layer. These SST effects are well resolved in the QuikSCAT observations but are underrepresented in the NWP wind fields (see the supporting online material in Chelton et al. 2004).

The comparisons between QuikSCAT, ECMWF, and NCEP wind speeds in section 5 concluded that there is no evidence of systematic errors in the NCEP wind speeds but there appear to be small but significant systematic errors in the ECMWF wind speeds. ECMWF wind speeds are biased low relative to NCEP wind speeds by about −0.4 m s^{-1}. A similar relative wind speed bias was inferred from comparisons of ECMWF speeds with those measured by 22 open-ocean buoys. The mean wind speed difference between the ECMWF 10-m winds and QuikSCAT 10-m equivalent

neutral stability winds is about -0.6 m s^{-1}, but decreases to about -0.4 m s^{-1} after adjustment for the effects of atmospheric stability. While it is difficult to eliminate systematic errors this small, such errors have a non-negligible effect on the wind-forced response in ocean general circulation models. As summarized in section 5, the apparent bias in the ECMWF wind speeds could lead to biases of 10%–20% in the wind stress magnitude.

Possible explanations for the random differences between scatterometer observations and contemporary NWP analyses of 10-m winds deduced from the results presented here include the limited spatial resolution of the models, inadequacies in the model parameterizations of the atmospheric boundary layer response to SST, and inaccuracies in the specification of the sea-surface temperature boundary condition (Chelton 2005). More detailed comparisons between the ECMWF and NCEP analyses and the QuikSCAT observations might yield additional insight into the nature of errors in present-day operational NWP analyses of 10-m winds, which could lead to further improvements in the models. This, in turn, would result in improved ECMWF- and NCEP-based estimates of air–sea fluxes of momentum, heat, and gases.

REFERENCES

Apel, J. R., 1994: An improved model of the ocean surface wave vector spectrum and its effects on radar backscatter. *J. Geophys. Res.,* **99,** 16 269–16 291.

Boukabara, S.-A., R. N. Hoffman, C. Grassotti, and S. M. Leidner, 2002: Physically based modeling of QuikSCAT SeaWinds passive microwave measurements for rain detection. *J. Geophys. Res.,* **107,** 4786, doi:10.1029/2001JD001243.

Chavanne, C., P. Flament, R. Lumpkin, B. Dousset, and A. Bentamy, 2002: Scatterometer observations of wind variations induced by oceanic islands: Implications for wind-driven ocean circulation. *Can. J. Remote Sens.,* **28,** 466–474.

Chelton, D. B., 2005: The impact of SST specification on ECMWF surface wind stress fields in the eastern tropical Pacific. *J. Climate,* in press.

——, M. H. Freilich, and S. K. Esbensen, 2000: Satellite observations of the wind jets off the Pacific coast of Central America. Part I: Case studies and statistical characteristics. *Mon. Wea. Rev.,* **128,** 1993–2018.

——, M. G. Schlax, M. H. Freilich, and R. F. Milliff, 2004: Satellite radar measurements reveal short-scale features in the wind stress field over the world ocean. *Science,* **303,** 978–983.

Cornillon, P., and K.-A. Park, 2001: Warm core ring velocities inferred from NSCAT. *Geophys. Res. Lett.,* **28,** 575–578.

Donelan, M., and W. J. Pierson, 1987: Radar scattering and equilibrium ranges in wind-generated waves with application to scatterometry. *J. Geophys. Res.,* **92,** 4971–5029.

Donnelly, W. J., J. R. Carswell, R. E. McIntosh, P. S. Chang, J. Wilkerson, F. Marks, and P. G. Black, 1999: Revised ocean backscatter models at C and Ku band under high wind conditions. *J. Geophys. Res.,* **104,** 11 485–11 497.

Draper, D. W., and D. G. Long, 2002: An assessment of SeaWinds on QuikSCAT wind retrieval. *J. Geophys. Res.,* **107,** 3212, doi:10.1029/2002JC001330.

Ebuchi, N., H. C. Graber, and M. J. Caruso, 2002: Evaluation of wind vectors observed by QuikSCAT/SeaWinds using ocean buoy data. *J. Atmos. Oceanic Technol.,* **19,** 2049–2062.

Freilich, M. H., 1997: Validation of vector magnitude datasets: Effects of random component errors. *J. Atmos. Oceanic Technol.,* **14,** 695–703.

——, and R. S. Dunbar, 1993: Derivation of satellite wind model functions using operational surface wind analyses: An altimeter example. *J. Geophys. Res.,* **98,** 14 633–14 649.

——, and ——, 1999: The accuracy of the NSCAT-1 vector winds: Comparisons with National Data Buoy Center buoys. *J. Geophys. Res.,* **104,** 11 231–11 246.

——, D. G. Long, and M. W. Spencer, 1994: SeaWinds: A scanning scatterometer for ADEOS II—Science overview. *Proc. Int. Geoscience and Remote Sensing Symp.,* Pasadena, CA, IEEE, 960–963.

Geernaert, G. L., F. Hansen, M. Courtney, and T. Herbers, 1993: Directional attributes of the ocean surface wind stress vector. *J. Geophys. Res.,* **98,** 16 571–16 582.

Grachev, A. A., S. W. Fairall, J. E. Hare, J. B. Edson, and S. D. Miller, 2003: Wind stress vector over ocean waves. *J. Phys. Oceanogr.,* **33,** 2408–2429.

Huddleston, J. N., and B. W. Stiles, 2000: Multidimensional histogram (MUDH) rain flag product description (version 3.0). Jet Propulsion Laboratory, Pasadena, CA, 8 pp. [Available online at ftp://podaac.jpl.nasa.gov/pub/ocean_wind/quikscat/L2B/doc/MUDH_Description_V3.pdf.]

Kelly, K. A., S. Dickinson, M. J. McPhaden, and G. C. Johnson, 2001: Ocean currents evident in satellite wind data. *Geophys. Res. Lett.,* **28,** 2469–2472.

Liu, W. T., and W. Tang, 1996: Equivalent neutral wind. JPL Publication 96-17, Pasadena, CA, 8 pp.

Mears, C. A., F. J. Wentz, and D. K. Smith, 2000: SeaWinds on QuikSCAT normalized objective function rain flag (version 1.2). Remote Sensing Systems, Santa Rosa, CA, 13 pp. [Available online at ftp://podaac.jpl.nasa.gov/pub/ocean_wind/quikscat/L2B/doc/NOF_Description_V1.2.pdf.]

——, D. K. Smith, and F. J. Wentz, 2001: Comparison of Special Sensor Microwave Imager and buoy-measured wind speeds from 1987 to 1997. *J. Geophys. Res.,* **106,** 11 719–11 729.

Milliff, R. F., J. Morzel, D. B. Chelton, and M. H. Freilich, 2004: Wind stress curl and divergence biases from rain effects on QuikSCAT surface wind retrievals. *J. Atmos. Oceanic Technol.,* **21,** 1216–1231.

Naderi, F. M., M. H. Freilich, and D. G. Long, 1991: Spaceborne radar measurement of wind velocity over the ocean—An overview of the NSCAT scatterometer system. *Proc. IEEE,* **97,** 850–866.

O'Neill, L. W., D. B. Chelton, and S. K. Esbensen, 2003: Observations of SST-induced perturbations of the wind stress field over the Southern Ocean on seasonal timescales. *J. Climate,* **16,** 2340–2354.

Pacanowski, R. C., 1987: Effect of equatorial currents on surface stress. *J. Phys. Oceanogr.,* **17,** 833–838.

Remund, Q. P., and D. G. Long, 2003: Large-scale inverse Ku-band backscatter modeling of sea ice. *IEEE Trans. Geosci. Remote Sens.,* **41,** 1821–1833.

Reynolds, R. W., K. Arpe, C. Gordon, S. P. Hayes, A. Leetmaa, and M. J. McPhaden, 1989: A comparison of tropical Pacific surface wind analyses. *J. Climate,* **2,** 105–111.

Rieder, K. F., J. A. Smith, and R. A. Weller, 1994: Observed directional characteristics of the wind, wind stress, and surface waves on the open ocean. *J. Geophys. Res.,* **99,** 22 589–22 596.

Smith, S. D., 1988: Coefficients for sea surface wind stress, heat flux, and wind profiles as a function of wind speed and temperature. *J. Geophys. Res.,* **93,** 15 467–15 472.

Stiles, B. W., and S. H. Yueh, 2002: Sea surface and winds—Impact of rain on spaceborne Ku-band wind scatterometer data. *IEEE Trans. Geosci. Remote Sens.,* **40,** 1973–1983.

Tournadre, J., and Y. Quilfen, 2003: Impact of rain cell on scatterometer data: 1. Theory and modeling. *J. Geophys. Res.,* **108,** 3225, doi:10.1029/2002JC001428.

Trenberth, K. E., W. G. Large, and J. G. Olson, 1990: The mean annual cycle in global ocean wind stress. *J. Phys. Oceanogr.,* **20,** 1742–1760.

Weissman, D. E., M. A. Bourassa, and J. Tongue, 2002: Effects of rain rate and wind magnitude on SeaWinds scatterometer wind speed errors. *J. Atmos. Oceanic Technol.,* **19,** 738–746.

Wentz, F. J., and R. W. Spencer, 1998: SSM/I rain retrievals within a unified all-weather ocean algorithm. *J. Atmos. Sci.,* **55,** 1613–1627.

Xie, S.-P., 2004: Satellite observations of cool ocean–atmosphere interaction. *Bull. Amer. Meteor. Soc.,* **85,** 195–208.

——, W. T. Liu, Q. Liu, and M. Nonaka, 2001: Far-reaching effects of the Hawaiian Islands on the Pacific ocean–atmosphere system. *Science,* **292,** 2057–2060.

Yueh, S. H., R. West, F. K. Li, W.-Y. Tsai, and R. Lay, 2000: Dual-polarized Ku-band backscatter signatures of hurricane ocean winds. *IEEE Trans. Geosci. Remote Sens.,* **38,** 73–88.